Recent Progress in the Analysis of Electromigration and Stress Migration in Large Multisegment Interconnects

Nestor Evmorfopoulos
Dept. of Electrical & Computer Engineering
University of Thessaly
Volos, Greece
nestevmo@uth.gr

Mohammad Abdullah Al Shohel
Dept. of Electrical & Computer Engineering
University of Minnesota
Minneapolis, MN (USA)
shohe001@umn.edu

Olympia Axelou
Dept. of Electrical & Computer Engineering
University of Thessaly
Volos, Greece
oaxelou@e-ce.uth.gr

Pavlos Stoikos
Dept. of Electrical & Computer Engineering
University of Thessaly
Volos, Greece
pastoikos@e-ce.uth.gr

Vidya. A. Chhabria
Dept. of Electrical & Computer Engineering
Arizona State University
Tempe, AZ, USA
vachhabr@asu.edu

Sachin S. Sapatnekar
Dept. of Electrical & Computer Engineering
University of Minnesota
Minneapolis, MN (USA)
sachin@umn.edu

ABSTRACT

Traditional approaches to analyzing electromigration (EM) in on-chip interconnects are largely driven by semi-empirical models. However, such methods are inexact for the typical multisegment lines that are found in modern integrated circuits. This paper overviews recent advances in analyzing EM in on-chip interconnect structures based on physics-based models that use partial differential equations, with appropriate boundary conditions, to capture the impact of electron-wind and back-stress forces within an interconnect, across multiple wire segments. Methods for both steady-state and transient analysis are presented, highlighting approaches that can solve these problems with a computation time that is linear in the number of wire segments in the interconnect.

CCS CONCEPTS

• **General and reference → Reliability**; • **Hardware → Metallic interconnect**; **Very large scale integration design**; **Electronic design automation**; **Physical design (EDA)**; **Aging of circuits and systems**.

KEYWORDS

Electromigration, stress, reliability, multisegment interconnects, steady-state analysis, transient analysis

ACM Reference Format:
Nestor Evmorfopoulos, Mohammad Abdullah Al Shohel, Olympia Axelou, Pavlos Stoikos, Vidya. A. Chhabria, and Sachin S. Sapatnekar. 2023. Recent Progress in the Analysis of Electromigration and Stress Migration in Large Multisegment Interconnects . In *Proceedings of the 2023 International Symposium on Physical Design (ISPD '23), March 26–29, 2023, Virtual Event, USA.* ACM, New York, NY, USA, 9 pages. https://doi.org/10.1145/3569052.3578919

ISPD '23, March 26–29, 2023, Virtual Event, USA

ACM ISBN 978-1-4503-9978-4/23/03…$15.00
https://doi.org/10.1145/3569052.3578919

1 INTRODUCTION

Electromigration (EM) is a very significant problem for current-day and future integrated circuits [1–3]. As wire widths have shrunk due to scaling (these width reductions are further exaggerated by the need to create cladding and capping layers in copper interconnects), the current densities in on-chip wires have increased tremendously. Moreover, while older technologies largely required EM checks in upper metal layers that carry the largest currents, in today's technologies, as transistors drive increasing amounts of current through narrow wires, EM is a bottleneck in lower metal layers [4, 5], potentially affecting a large number of on-chip wire segments.

The conventional method for EM analysis for interconnects involves a two-stage process. In the first stage, immortal wires are filtered out using the Blech criterion [6], which recognizes that stress in a metal wire can settle to a steady-state value due to the counterplay between the electric field and the back-stress. In the second stage, potentially mortal wires undergo further analysis using the semi-empirical Black's equation to check whether or not the EM failure may occur during the product lifespan [7]. The limits used in each check are typically characterized on test structures with a single segment and extrapolated to multisegment lines. To overcome the limitations of these models, there has been increasing interest in using physics-based analysis for EM in interconnects. The roots of such analysis lies in decades-old work by [8–10], and culminated in the work of Korhonen *et al.* in [11], which presented a canonical treatment of EM equations in a metallic interconnect, with solutions for a semi-infinite and finite line. These results were further refined for single-segment lines in [12, 13] by using an infinite series solution to the equations to predict EM failures.

The EM solution for single-segment lines does not carry over to multisegment lines. Consider the two-segment structure of Fig. 1(a), with current densities of $j_1 = j$ and $j_2 = 2j$ in the two segments, where $w_1 = w_2 = w$, and $l_1 = l_2 = l$. In [14], it was observed that the time-to-failure of the segment with the lower current density

was shorter, and the discrepancy was explained by stating that the underlying cause is that Segment 1 provides atomic flux to Segment 2, leading to higher depletion at its cathode. Empirical approaches fail to capture this stress accumulation, but physics-based methods do so. The steady-state stress profile obtained from Korhonen's equation is shown in Fig. 1(b), using notation to be defined in Section 2: even though the segment at right has lower current density, it experiences higher stress, $\sigma(x)$ at its right end, due to the accumulation of stress over the two segments.

Analogous to the traditional semi-empirical methodology, physics-based EM approaches must solve two types of problems:
(1) The *steady-state analysis* problem considers the case when all transients have settled, and determines the steady-state stress in the wire. If this stress is below the critical stress for void formation, the wire is considered to be immortal. This analysis can be seen as a generalization of the Blech criterion, which solves the steady-state analysis problem for a single-segment wire. By filtering out immortal wires [15], the number of wires that must be considered for more detailed analysis is reduced to a more manageable number.
(2) The *transient analysis* problem is solved on potentially mortal wires (which pass the above immortality filter), and determines the evolution of stress as a function of time in these wires. This solution is obtained by solving Korhonen's equation, together with the corresponding boundary conditions, over time and over all segments in a multisegment interconnect. While Korhonen's equation provides the time to void formation, during the post-voiding phase that follows, it is possible for a wire to remain functional. A modification to Korhonen's equation that accounts for void formation was proposed in [16] and numerical solutions based on the so-called extended Korhonen model (EKN) were provided in [17].

Early methods for solving for EM failure on large structures [13, 15, 18–20], such as multisegment interconnects with a large number of segments, were either computationally expensive or insufficiently accurate. However, there has been a great deal of progress in recent years that enables the accurate analysis of the transient and steady-state analysis problems with a computation time that is linear in the number of segments. In this paper, we present an overview of methods that perform fast analysis of large multisegment interconnects. In Section 2, we present the physics-based formulation for EM. Sections 3 and 4 overview recent progress in solving the steady-state and transient EM problems, respectively, and we conclude the paper in Section 5.

2 BACKGROUND

2.1 Korhonen's Equation

Fig. 2 shows the cross-section of a Cu dual-damascene (DD) wire and illustrates the electromigration mechanism in terms of two driving forces i.e. the electron wind force and the back-stress force. When current flows in the wire, the momentum of the electrons drive metal atoms from the cathode towards the anode, in the direction of electron flow. The movement of migrating atoms is limited to a single metal layer since the barrier layer acts as a blocking boundary for mass transport [21, 22] and prevents atoms from migrating to other metal layers. Due to this electron wind force, the cathode is depleted of metal atoms and a tensile stress is built up near the cathode, which may lead to void formation.

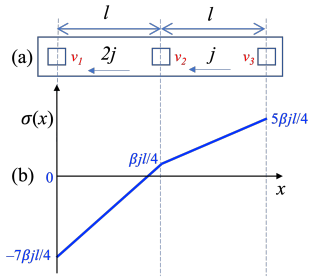

Figure 1: (a) A two-segment interconnect topology. (b) The results of a physics-based analysis of its steady-state stress.

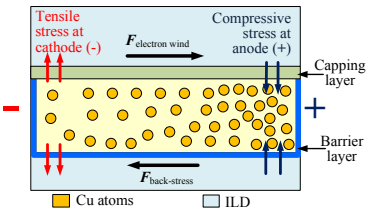

Figure 2: Illustration of electromigration in a Cu wire [15].

Simultaneously, migrating atoms accumulate at the anode terminal and a compressive stress is created near the anode. As metal atoms migrate towards the anode, the resulting concentration gradient (sometimes referred to in the literature as the chemical potential gradient) creates a stress-induced reverse flow of atoms to the cathode. This force, which acts against the electron wind force, is proportional to the stress gradient and known as back-stress force.

A single interconnect segment injects electron current from the cathode towards the anode. Since the length of a wire is typically much larger than the other two dimensions, the temporal evolution of EM-induced stress, $\sigma(x,t)$, at any point in the segment is modeled by the 1–D partial differential equation (PDE) [11] that relates the stress σ to x, the distance from the cathode:

$$\frac{\partial \sigma}{\partial t} = \frac{\partial}{\partial x}\left[\kappa\left(\frac{\partial \sigma}{\partial x} + \beta j\right)\right] \tag{1}$$

Here, $\beta = Z^* e\rho/\Omega$, and $\kappa = D_a \mathcal{B}\Omega/(kT)$, where j is the current density through the wire, Z^* is the effective charge number, e is the electron charge, ρ is the resistivity, Ω is the atomic volume for the metal, $\mathcal{B}$ is the bulk modulus of the material, k is Boltzmann's constant, T is the temperature, and $D_a = D_0 e^{-E_a/kT}$ is the diffusion coefficient, with E_a being the activation energy.

As in [11], the sign convention for j is in the direction of electron current, i.e., opposite to conventional current and the electric field. There are two terms on the right hand side of (1). The second term, βj, represents atomic flux attributable to the electron wind force, while the first term containing the stress gradient $\partial\sigma/\partial x$ accounts for the flux related to the back-stress force. The sum, $(\partial\sigma/\partial x + \beta j)$, is proportional to the net atomic flux.

2.2 Equations for a Multisegment Interconnect

A general interconnect structure consists of a set of *segments* of wires between vias and junctions, each associated with a current density. In general, for a multisegment interconnect structure, currents may be injected (or drawn) at intermediate nodes through

vias. For an intermediate node n_i of the structure with degree d_i, we denote the set of incident segments as $S_i = \{s_1, s_2, \cdots, s_{d_i}\}$.

Stress evolution in each segment is described by the partial differential equation (1). These equations are supplemented by a set of boundary conditions (BCs) that relate the stress at various segments, and a temporal boundary condition that initializes the segment stresses to zero at $t = 0$. The spatial boundary conditions, which must be obeyed over all time points, are as follows [17]:
(1) Continuity constraints: At any intermediate node, the stress must be continuous. For each segment s_k incident on node n_i, if $\sigma_{s_k}|_{n_i}$ is its stress at n_i, then

$$\sigma_{s_1}|_{n_i} = \sigma_{s_2}|_{n_i} = \cdots = \sigma_{s_{d_i}}|_{n_i} \tag{2}$$

(2) Flux constraints: The net atomic flux entering each node n_i must sum to zero, i.e.,

$$\sum_{s_k \in S_i} w_{s_k} \tau_{s_k} \left(\frac{\partial \sigma_{s_k}}{\partial x}\bigg|_{n_i} + \beta j_{s_k} \right) = 0 \tag{3}$$

where S_i is the set of segments incident on n_i. The term j_{s_k} is the current density through segment s_k, which is positive when directed away from n_i and negative when directed into n_i, and w_{s_k} and τ_{s_k} are, respectively, the segment width and thickness.
For a line with uniform width and thickness, this condition becomes:

$$\left(\frac{\partial \sigma_{s_i}}{\partial x}\bigg|_{n_i} + \beta j_{s_i} \right) = \left(\frac{\partial \sigma_{s_{i+1}}}{\partial x}\bigg|_{n_i} + \beta j_{s_{i+1}} \right) \tag{4}$$

for every node n_i connecting segments s_i and s_{i+1}.
A special case of condition (3) is that at any end-point (terminal) node n_i of the structure with degree 1, the boundary conditions dictate that there is zero atomic flux through the boundaries at the end points over all time, i.e.,

$$\frac{\partial \sigma}{\partial x}\bigg|_{n_i} + \beta j_s = 0 \tag{5}$$

where j_s is the current density in the segment s incident on n_i.
(3) Mass conservation constraint: Finally, the total flux over the entire interconnect must be conserved:

$$\sum_{\text{all segments } s_k} \iiint \sigma_{s_k}(x)\, dx\, dw\, d\tau = 0 \tag{6}$$

where $\sigma_{s_k}(x)$ is the stress at location x in segment s_k. The triple integral is taken over the volume of each segment s_k.

3 STEADY-STATE ANALYSIS

When the electron wind and back-stress forces reach equilibrium in the steady state, then for each segment i, over its entire length,

$$\frac{\partial \sigma_i}{\partial x} + \beta j_i = 0, \text{ i.e., } \frac{\partial \sigma_i}{\partial x} = -\beta j_i \tag{7}$$

Thus, after all transients have dissipated, the stress varies linearly along a segment, with a gradient of the stress that is proportional to the segment current density, as observed in [23–26].

The Blech immortality criterion for a single-segment line asserts that if the maximum steady-state stress falls below the critical stress, σ_{crit}, required to nucleate a void, then the wire is considered immortal. This translates to the check [6]:

$$jl \le (jl)_{crit} \tag{8}$$

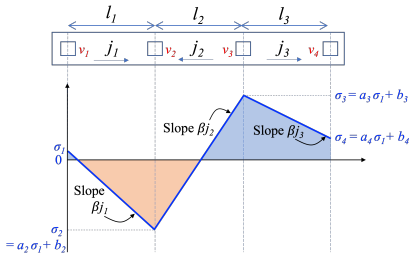

Figure 3: A three-segment example to illustrate the intuition behind fast steady-state computation.

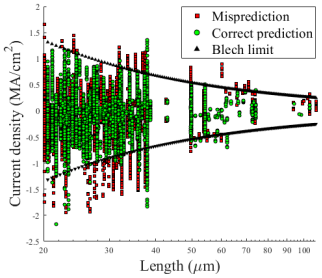

Figure 4: Inaccuracy of the traditional Blech filter for the ibmpg6 benchmark [30].

where $(jl)_{crit}$ is a function of the critical stress, σ_{crit}.

For a general multisegment interconnect, the stress function is continuous at segment boundaries (Eq. (2)) and the stress varies linearly along the wire, as shown for a three-segment interconnect in Fig. 3. The steady-state stresses can be represented by a set of difference equations [27–29]. The steady-state stresses at the two ends of edge e_k, directed from node a to node b, are related by:

$$\sigma^b - \sigma^a = -\beta j_k l_k \tag{9}$$

If we know the stress σ_1 at the left end of a multisegment interconnect line without branches, every node stress can be analytically computed in terms of σ_1. To find σ_1, we can apply the mass conservation constraint (6); this yields all stresses in the line.

In [29], a current-based formulation was presented, using the fact that the stress difference across a wire segment is a function of its current. For tree topologies, it was shown that the stress computation can be performed through a linear-time tree traversal, which is both fast and very inexpensive in its memory footprint; furthermore, it was shown that for any mesh, it is adequate to analyze a spanning tree because the total "stress drop" around any cycle is zero for the currents in the network at any point in time.

Fig. 4 [30] plots the current density j vs. the wire length l within the segments of the ibmpg6 benchmark in Cu DD technology. The currents in the Vdd and Vss lines may be either positive or negative, and their magnitude affects EM. The black triangles show the contours of $jl = (jl)_{crit}$: when the magnitude lies within this frontier for a segment of the grid, the traditional Blech criterion (8) would label the wire as immortal; otherwise it is potentially mortal. The figure shows green markers for correct predictions and red markers for incorrect predictions. It is immediately obvious that the Blech criterion shows significant inaccuracy on multisegment wires, but since the figure shows the 1.6M edges of the ibmpg6

benchmarks, the scatter points of several segments are hidden due to overlaps. Quantitatively, 29% of the predictions from the Blech criterion are inaccurate. The root cause for such mispredictions can be understood based on the qualitative description in Fig. 1.

An alternative voltage-based formulation has been proposed in [26], but its potential for linear-time computation was not realized in this work as it was applied to a set of very small test structures. This formulation was used again in [31], and applied to a wider set of structures, but their results show a quadratic to cubic growth in runtime with problem size. In [28], the voltage-based formulation was shown to admit a linear-time stress computation by relating the steady-state stress at a node to its voltage. An alternative formulation of the same voltage-based formulation was presented in [30]: this exposition directly relates the current-based formulation to the voltage-based formulation.

For mesh structures, the above techniques are applicable for the case where all branch currents are specified in a way that satisfies Kirchhoff's voltage law (KVL), with zero net voltage drop across any cycle. However, in EM analysis, it is possible that the inputs are provided in the form of worst-case currents. The net voltage drop across any cycle is zero at a given time instant, but since these worst-case currents can occur at different times, it is possible that the summation of the current-resistance products across a cycle may not be zero. In this case, the method in [29] can be adapted by choosing a worst-case tree that results in the largest stress. In contrast, voltage-based methods, which depend on KVL, cannot directly capture this scenario.

4 TRANSIENT ANALYSIS

4.1 Analytical Solutions for Multisegment Lines

Transient analysis attempts to calculate the temporal evolution of stress by solving Korhonen's equation (1) with the appropriate boundary conditions for the given interconnect structure. For a line with multiple segments (such as those typically found in power grids), the analytical calculation of stress involves finding the general solution of (1) with appropriate unknown constants in every line segment, and then applying the BCs (2)-(5) to assemble and solve (symbolically) the resulting algebraic system of equations in the unknown constants (which are twice as many as the number of segments). Until recently, this has only been possible for very small structures of up to four segments [13, 18], beyond which the size and complexity of symbolic algebraic equations to be assembled and solved becomes prohibitive.

The work in [32] is the first to provide fully analytical solutions of stress for lines with an arbitrary number of segments. This is achieved by ascribing a novel wave-kind physical analogy to stress. Specifically, at every via where current is drawn from or injected to the line, there is a source of stress flux $\partial\sigma/\partial x$ that generates buildup of stress along the line[1]. This stress buildup can be thought of as a wave that starts from the sources and travels along the line, undergoing reflections at the line terminals which are then superposed to the fundamental waves and lesser-order reflections (analogous to multiple interfering "stress waves").

[1]Since Korhonen's equation is a PDE similar to the heat or diffusion equation, the source of stress flux will be like injecting a prescribed heat flux or flux of a diffusant at the point of the via.

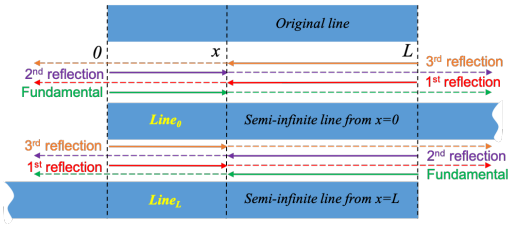

Figure 5: A single-segment line illustrating fundamentals and three reflections of stress flux originating at side boundaries.

To explain the concept behind the method of [32], consider first two semi-infinite lines from $x = 0$ to $+\infty$, and from $x = L$ to $-\infty$, carrying currents with constant density j. At location x at time t, the solution to the stress equation is derived in [11] and [32] respectively as:

$$\sigma(x,t) = G\cdot g(x,t) \tag{10}$$

$$\sigma(x,t) = -G\cdot g(L-x,t) \tag{11}$$

$$\text{where } g(x,t) = 2\sqrt{\frac{\kappa t}{\pi}}\exp\left(-\frac{x^2}{4\kappa t}\right) - x\cdot\operatorname{erfc}\left(\frac{x}{2\sqrt{\kappa t}}\right) \tag{12}$$

with $G = \beta j$, and $\operatorname{erfc}(x) = \frac{2}{\sqrt{\pi}}\int_x^\infty e^{-t^2}dt$ being the complementary error function.

Consider now a finite single-segment line of length L that injects current with density j from the cathode terminal to the anode terminal. It is shown in [32] (using the Laplace transform of (1) and (5) along with some clever use of geometric series expansion) that the solution for the stress at location x at time t takes the form of the infinite series[2]:

$$\sigma(x,t) = G\sum_{n=0}^{\infty}(-1)^n[g(nL+x,t) - g((n+1)L-x,t)] \tag{13}$$

The terms $G\cdot g(x,t)$ and $-G\cdot g(L-x,t)$ that result by taking $n = 0$ in (13) are the exact solutions (10) and (11) of the semi-infinite lines from 0 to $+\infty$ (where the distance from the left edge is x), and from L to $-\infty$ (where the distance from the right edge to x is $L - x$). These can be considered as *fundamentals* of two sources of stress flux equal to $\partial\sigma/\partial x = -G$ originating at the boundaries $x = 0$ and $x = L$, traveling down in semi-infinite lines of opposite directions.

Now for $n = 1$ the resulting terms $G\cdot g(2L-x,t)$ and $-G\cdot g(L+x,t)$ can be regarded as *reflections* of the aforementioned fundamentals at the opposite boundaries, which then travel back to the variable point x and are superposed to the original fundamentals. Specifically, the term $G\cdot g(2L-x,t)$ is the fundamental originating at $x = 0$ after being reflected at $x = L$ and going back at x (traveling total distance $L + (L - x) = 2L - x$), while $-G\cdot g(L+x,t)$ is the fundamental originating at $x = L$ after being reflected at $x = 0$ and going back at x (traveling total distance $L + x$).

Analogously for $n = 2$, the term $G\cdot g(2L+x,t)$ is the fundamental from $x = 0$ after two reflections (at $x = L$ and then at $x = 0$) before traveling to location x (having traveled distance $2L + x$), while $-G\cdot g(3L-x,t)$ is the fundamental from $x = L$ after reflections at $x = 0$ and then $x = L$ before going back to location x (having traveled distance $2L + (L - x) = 3L - x$).

[2]This is a different infinite series solution than the one obtained by the method of Separation of Variables and which was originally given in [11].

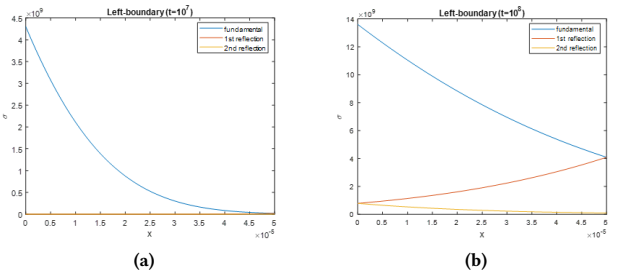

Figure 6: Plots of fundamental and first two reflections of stress flux at $x = 0$ in a single-segment line, as functions of the distance from the source, for times (a) $t = 10^7 s$, (b) $t = 10^8 s$.

The fundamentals along with reflections of up to third order are illustrated in Fig. 5 for the single-segment line. Higher-order reflections are obtained from (13) for larger values of n. By this conceptual process we can build up the entire infinite series solution, but in practice only a small number of terms suffices for near-perfect approximation since the function (12) decreases exponentially with distance (while it only increases weakly with time). This is demonstrated in Fig. 6 where reflections of order as low as 2nd are typically negligible, and they only become appreciable for very large times (reflections of order greater than 2nd can be safely ignored in nearly all practical cases).

The wave-like view of fundamentals and reflections enables the construction of analytical expressions of stress for lines with an arbitrary number of segments. Consider the case of a two-segment finite line (illustrated in Fig. 7), consisting of one segment from $x = 0$ to $x = L_1$ with current density j_1 and another from $x = L_1$ to $x = L_2$ with current density j_2. The via at the intersection $x = L_1$ draws from or injects current to the line, so that $j_1 \neq j_2$. At $x = L_1$, the line must obey boundary conditions (2) and (4) that enforce the continuity of stress and continuity of atomic flux respectively.

The sources of stress flux $\partial\sigma/\partial x = -G_1$ at $x = 0$, and $\partial\sigma/\partial x = -G_2$ at $x = L_2$ (where $G_1 = \beta j_1, G_2 = \beta j_2$) are handled in exactly the same way as the single-segment line, by considering fundamentals and successive reflections at the two boundaries. At the intersection $x = L_1$, the boundary condition (4) indicates that there is a discontinuity in the stress gradient equal to $\frac{\partial\sigma_1}{\partial x} - \frac{\partial\sigma_2}{\partial x} = G_2 - G_1$ (due to the current being injected or drawn at the via there). This acts as another source of stress flux, creating two fundamental components that travel sideways from $x = L_1$ and along the semi-infinite parts of a two-segment infinite line, i.e. from $x = L_1$ to $+\infty$ and from $x = L_1$ to $-\infty$. It was shown in [32] that the fundamental traveling left (for $x < L_1$) is $\frac{G_2-G_1}{2} g(L_1 - x, t)$, while the fundamental traveling right (for $x > L_1$) is $\frac{G_2-G_1}{2} g(x - L_1, t)$.

Like the fundamentals originating at the boundaries, the fundamentals originating at $x = L_1$ are also reflected at the boundaries $x = 0$ and $x = L_2$. Specifically, the leftward traveling fundamental undergoes a 1st reflection at $x = 0$ before arriving (again or for the first time) at location x (having traveled distance $L_1 + x$), then a 2nd reflection at the boundary $x = L_2$ before arriving once again at x (with distance traveled $L_1 + L_2 + (L_2 - x) = L_1 + 2L_2 - x$), and so on. The rightward traveling fundamental undergoes a 1st reflection at $x = L_2$ before arriving (again or for the first time) at location x (having traveled distance $(L_2 - L_1) + (L_2 - x) = -L_1 + 2L_2 - x$),

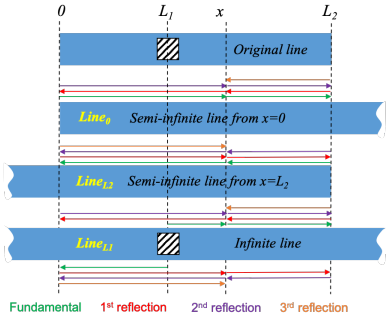

Figure 7: A two-segment line illustrating fundamentals and first three reflections of stress flux originating at the side boundaries and the intersection point.

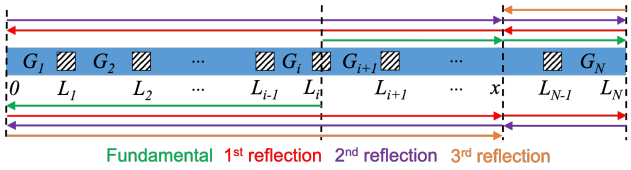

Figure 8: Fundamental and first three reflections of stress flux originating at an intermediate via for an N-segment line.

then a 2nd reflection at $x = 0$ before arriving once again at x (with distance traveled $(L_2 - L_1) + L_2 + x = -L_1 + 2L_2 + x$), and so on.

Taking the superposition of fundamentals and reflections of up to 2nd-order for all sources of stress flux, one can construct the following analytical approximation of stress for the two-segment line that gives almost perfect accuracy:

$$\begin{aligned}\sigma(x,t) \approx\ & G_1\left[g(x,t) + g(2L_2 - x, t) + g(2L_2 + x, t)\right] \\ & - G_2\left[g(L_2 - x, t) + g(L_2 + x, t) + g(3L_2 - x, t)\right] \\ & + \frac{G_2 - G_1}{2}\left[g(|L_1 - x|, t) + g(L_1 + x, t)\right. \\ & \quad + g(L_1 + 2L_2 - x, t) + g(-L_1 + 2L_2 - x, t) \\ & \quad \left. + g(-L_1 + 2L_2 + x, t)\right] \end{aligned} \tag{14}$$

The above expression can be easily adapted to include more reflections if needed. In fact, if all reflections up to infinite order are included, it can be shown [32] that the resulting expression exactly matches the full infinite series solution. However, reflections of order higher than 2nd are hardly ever necessary in practice.

The described concept of constructing the solution in a wave-like fashion, by source fundamentals and reflections, can be straightforwardly extended to a line with an arbitrary number of segments. Consider a multisegment line of length L_N (illustrated in Fig. 8) being composed of N line segments with parameters G_1 to G_N (corresponding to current densities j_1 to j_N) and intersection points at locations $x = L_1$ to $x = L_{N-1}$ (where the length of the k^{th}-segment is $L_k - L_{k-1}$). The analytical approximation of stress will be a straightforward generalization of (14), consisting of the fundamentals from the two boundaries $x = 0$ and $x = L_N$ and the $N - 1$ intersection points, along with their reflections of up to 2nd order

(which are more than sufficient in practice):

$$\begin{aligned}\sigma(x,t) \approx\ & G_1\left[g\left(x,t\right)+g\left(2L_N-x,t\right)+g\left(2L_N+x,t\right)\right]\\ & -G_N\left[g\left(L_N-x,t\right)+g\left(L_N+x,t\right)+g\left(3L_N-x,t\right)\right]\\ & +\sum_{i=1}^{N-1}\frac{G_{i+1}-G_i}{2}\left[g\left(\left|L_i-x\right|,t\right)+g\left(L_i+x,t\right)\right.\\ & \qquad +g\left(L_i+2L_N-x,t\right)+g\left(-L_i+2L_N-x,t\right)\\ & \qquad \left.+g\left(-L_i+2L_N+x,t\right)\right] \end{aligned} \tag{15}$$

where $g(.)$ is the function defined in (12). The above expression can be easily adapted to include more (or fewer) reflected terms, and even different number of reflected terms for each individual source.

The work in [32] reports the solution of EM stress, using the above analytical expression (15), for entire power grids with approximately 200K segments in only a few seconds, and with perfect accuracy against commercial numerical solvers like COMSOL. Results also demonstrate significant pessimism of steady state predictions vs. the actual EM failures at the end of chip lifetime. The present challenge is to extend the described reflections framework and stress-wave analogy to more general interconnect structures.

4.2 Semi-Analytical Solutions for Multisegment Lines

Semi-analytical approaches for transient analysis discretize the PDE (1) in one independent variable (either the spatial or the temporal one) while keeping the other continuous. Keeping time continuous here is much more important as it allows the calculation of stress at any future time directly (especially for long chip lifetimes in the order of decades, which can render numerical time integration completely prohibitive). On the other hand, spatial discretization is much less of an issue, because even in fully analytical methods we still compute stress at specific discrete spatial points.

The work in [33] presents a semi-analytical approach that can calculate stress for any future time in an arbitrary N-segment line, providing a simple closed-form matrix equation which can be evaluated in $O(n \log n)$ computational time (where n is the number of discretization points). Fig. 9 shows an example of a two-segment line discretized in the spatial coordinate with step Δx into $n = 6$ discrete points (two non-physical or ghost points are also shown, which are solely used for application of the blocking BCs (5) at the line terminals).

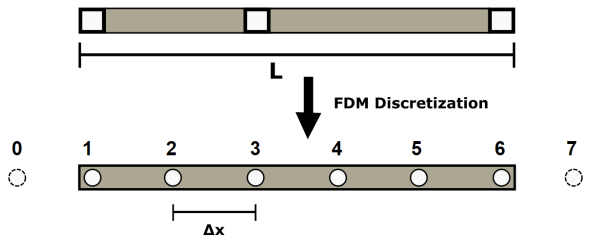

Figure 9: A two-segment line and its spatial discretization.

A finite-difference-method (FDM) approximation of the spatial derivative in (1), for any discretization point $i = 1, \ldots, n$ (other than via points) of the line, results in:

$$\begin{aligned}\frac{d\sigma_i}{dt} \equiv \dot{\sigma}_i &= \kappa\frac{\left(\frac{\sigma_{i+1}-\sigma_i}{\Delta x}\right)-\left(\frac{\sigma_i-\sigma_{i-1}}{\Delta x}\right)}{\Delta x}\\ &= \frac{\kappa}{\Delta x^2}\left(\sigma_{i+1}-2\sigma_i+\sigma_{i-1}\right)\end{aligned} \tag{16}$$

The equations for the endpoints $i = 0$ and $i = n$ are obtained by eliminating, in (16), the ghost points through the FDM approximations of the terminal BCs (5). The latter become for $i = 0$ and $i = n$ respectively:

$$\frac{\sigma_1-\sigma_0}{\Delta x}+\beta j_1=0; \qquad \frac{\sigma_{n+1}-\sigma_n}{\Delta x}+\beta j_N=0 \tag{17}$$

Note that the spatial derivatives in (5) are approximated in the direction of increasing x (the convention used in [11] is that x increases in the direction of electron current, i.e. opposite to the conventional current). By applying (16) for $i = 1$ and $i = n$, and eliminating σ_0 and σ_{n+1} from (17), the FDM equations for σ_1 and σ_n become:

$$\begin{aligned}\dot{\sigma}_1 &= \frac{\kappa}{\Delta x^2}\left(\sigma_2-\sigma_1\right)+\frac{\kappa}{\Delta x}\beta j_1\\ \dot{\sigma}_n &= \frac{\kappa}{\Delta x^2}\left(-\sigma_n+\sigma_{n-1}\right)-\frac{\kappa}{\Delta x}\beta j_N\end{aligned} \tag{18}$$

For the via intersection points, since adjacent discretization points belong to segments with different current densities, the FDM equations result by spatially discretizing (1) while simultaneously applying the continuous-flux BCs (4). Specifically, for a via point i with adjacent points $i-1$ and $i+1$ belonging to segments k and $k+1$, the FDM equation is:

$$\dot{\sigma}_i = \frac{\kappa}{\Delta x^2}\left(\sigma_{i-1}-2\sigma_i+\sigma_{i+1}\right)+\frac{\kappa}{\Delta x}\beta(j_{k+1}-j_k) \tag{19}$$

Writing the FDM equations for all discrete points from (16), (18), and (19), the following system of ordinary differential equations (ODEs) is obtained:

$$\begin{bmatrix}\dot{\sigma}_1\\ \dot{\sigma}_2\\ \vdots\\ \dot{\sigma}_{n-1}\\ \dot{\sigma}_n\end{bmatrix} = \frac{\kappa}{\Delta x^2}\begin{bmatrix}-1 & 1 & 0 & \cdots & 0 & 0\\ 1 & -2 & 1 & \cdots & 0 & 0\\ \vdots & \vdots & \ddots & \ddots & \vdots & \vdots\\ 0 & 0 & \cdots & 1 & -2 & 1\\ 0 & 0 & \cdots & 0 & 1 & -1\end{bmatrix}\begin{bmatrix}\sigma_1\\ \sigma_2\\ \vdots\\ \sigma_{n-1}\\ \sigma_n\end{bmatrix}+\frac{\kappa\beta}{\Delta x}\mathbf{D}\begin{bmatrix}j_1\\ \vdots\\ j_N\end{bmatrix} \tag{20}$$

where $\mathbf{D}$ is an $n \times N$ matrix with elements $d_{11} = 1$, $d_{nN} = -1$, and $d_{ik} = -1$, $d_{i,k+1} = 1$ for the discrete points i that connect segments k and $k+1$ (and zeros everywhere else). For example, the matrix $\mathbf{D}$ for the six-point two-segment wire of Fig. 9 is:

$$\mathbf{D} = \begin{bmatrix}1 & 0\\ 0 & 0\\ -1 & 1\\ 0 & 0\\ 0 & 0\\ 0 & -1\end{bmatrix} \tag{21}$$

The ODE system (20) has the familiar form of a linear time-invariant (LTI) system:

$$\dot{\boldsymbol{\sigma}}(t) = \mathbf{A}\boldsymbol{\sigma}(t)+\mathbf{B}\mathbf{j} \tag{22}$$

with $\mathbf{B} = \frac{\kappa\beta}{\Delta x}\mathbf{D}$ and:

$$\mathbf{A} = \frac{\kappa}{\Delta x^2}\begin{bmatrix} -1 & 1 & 0 & \cdots & 0 & 0 \\ 1 & -2 & 1 & \cdots & 0 & 0 \\ \vdots & \vdots & \ddots & \ddots & \vdots & \vdots \\ 0 & 0 & \cdots & 1 & -2 & 1 \\ 0 & 0 & \cdots & 0 & 1 & -1 \end{bmatrix} \tag{23}$$

The analytical solution of (22) can be obtained as the convolution integral:

$$\boldsymbol{\sigma}(t) = e^{\mathbf{A}t}\boldsymbol{\sigma}(0) + \int_0^t e^{\mathbf{A}(t-\tau)}\,\mathbf{B}\mathbf{j}\,d\tau \tag{24}$$

where $\boldsymbol{\sigma}(0)$ is the vector of initial stress conditions at the n discretization points.

If $\mathbf{A} = \mathbf{V}\Lambda\mathbf{V}^{-1}$ is the eigendecomposition of $\mathbf{A}$, then it is well-known that $e^{\mathbf{A}t} = \mathbf{V}e^{\Lambda t}\mathbf{V}^{-1}$, and thus (24) becomes (assuming, without loss of generality, that $\boldsymbol{\sigma}(0) = \mathbf{0}$):

$$\boldsymbol{\sigma}(t) = \int_0^t \mathbf{V}e^{\Lambda(t-\tau)}\mathbf{V}^{-1}\mathbf{B}\mathbf{j}\,d\tau = \mathbf{V}\left(\int_0^t e^{\Lambda(t-\tau)}\,d\tau\right)\mathbf{V}^{-1}\mathbf{B}\mathbf{j} \tag{25}$$

Since Λ is diagonal, the matrix integral in the above equation has the form:

$$\int_0^t e^{\Lambda(t-\tau)}\,d\tau = \begin{bmatrix} \int_0^t e^{\lambda_1(t-\tau)}\,d\tau & & \\ & \ddots & \\ & & \int_0^t e^{\lambda_n(t-\tau)}\,d\tau \end{bmatrix} \tag{26}$$

where λ_j, $j = 1, \ldots, n$ are the (not generally distinct) eigenvalues of $\mathbf{A}$. Each of the above integrals can be computed analytically as:

$$\int_0^t e^{\lambda_j(t-\tau)}\,d\tau = \left[-\frac{e^{\lambda_j(t-\tau)}}{\lambda_j}\right]_{\tau=0}^{\tau=t} = \frac{e^{\lambda_j t} - 1}{\lambda_j} \tag{27}$$

Note that if one eigenvalue equals zero, then the corresponding integral is simply $\int_0^t d\tau = t$.

Now, for the specific matrix $\mathbf{A}$ with the form (23), it was shown in [34] that its eigendecomposition can be determined beforehand. Specifically, $\mathbf{A}$ has n distinct eigenvalues which are given by:

$$\lambda_j = \frac{\kappa}{\Delta x^2}\left(2\cos\frac{(j-1)\pi}{n} - 2\right), \quad j = 1, \ldots, n \tag{28}$$

while its eigenvectors are orthonormal (satisfying $\mathbf{V}^{-1} = \mathbf{V}^T$) and are such that the products $\mathbf{V}^T\mathbf{r}$ and $\mathbf{V}\mathbf{r}$ of the matrices $\mathbf{V}^T$,$\mathbf{V}$ with an arbitrary vector $\mathbf{r}$ amount to performing respectively a Discrete Cosine Transform of type-II (DCT-II) and an Inverse Discrete Cosine Transform of type-II (IDCT-II) [35] on $\mathbf{r}$. Both of these can be computed with near-linear complexity $O(n \log n)$ (instead of the quadratic complexity $O(n^2)$ of general matrix-vector products) using Fast Fourier Transform, in a fashion similar to a fast Poisson solver like [36] in one dimension.

By inserting (27) into (25), the following analytical solution for stress at any given time for the pre-selected discrete points of a multisegment line is obtained:

$$\boldsymbol{\sigma}(t) = \mathbf{V}\mathbf{L}(t)\mathbf{V}^T\mathbf{B}\mathbf{j} \tag{29}$$

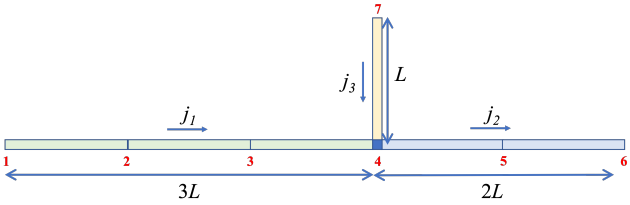

Figure 10: A three-segment tree and its spatial discretization.

where:

$$\mathbf{L}(t) = \begin{bmatrix} t & & \\ & \frac{e^{\lambda_2 t}-1}{\lambda_2} & \\ & & \ddots \\ & & \frac{e^{\lambda_n t}-1}{\lambda_n} \end{bmatrix} \tag{30}$$

and λ_j, $j = 2, \ldots, n$ are given by (28), while the matrix-vector products are computed through DCT-II/IDCT-II in $O(n \log n)$ time. The work in [33] has used the above expression to simulate EM stress in the largest of IBM power grid benchmarks [37], with over 1M line segments, for a time of 20 years in the future in only a few seconds.

4.3 Semi-Analytical Solutions for Interconnect Trees

While power grid lines are considerably more susceptible to EM due to the flow of large unidirectional currents, EM is becoming increasingly important in signal interconnect trees carrying bidirectional currents [38]. For interconnect trees, a similar semi-analytical approach to the one presented in Section 4.2 can be formulated, which discretizes only space while keeping time continuous. The FDM approximations (16) and (18) for internal discretization points and terminal points still hold. The additional complication for trees are the equations for junctions (with or without vias).

Considering the simple three-segment interconnect tree of Fig. 10 as an example, at the junction point $i = 4$ the FDM equation is obtained by taking the sum of finite difference approximations for the spatial derivatives along the three directions, while approximating the temporal derivative of stress along each incident discrete segment by the average of the temporal derivatives at its endpoints[3]. The net result is:

$$\frac{3}{2}\dot{\sigma}_4 = \frac{\kappa}{\Delta x^2}(\sigma_3 + \sigma_5 + \sigma_7 - 3\sigma_4) + \frac{\kappa}{\Delta x}\beta(-j_1 + j_2 - j_3) \tag{31}$$

Writing the equations for the other discrete points $i = 1$ to $i = 7$ of the tree, the following system of ODEs is obtained:

[3]This is analogous to the familiar π-model approximation of discrete segments in distributed RC networks

$$\begin{bmatrix} \frac{1}{2} & 0 & 0 & 0 & 0 & 0 & 0 \\ 0 & 1 & 0 & 0 & 0 & 0 & 0 \\ 0 & 0 & 1 & 0 & 0 & 0 & 0 \\ 0 & 0 & 0 & \frac{3}{2} & 0 & 0 & 0 \\ 0 & 0 & 0 & 0 & 1 & 0 & 0 \\ 0 & 0 & 0 & 0 & 0 & \frac{1}{2} & 0 \\ 0 & 0 & 0 & 0 & 0 & 0 & \frac{1}{2} \end{bmatrix} \begin{bmatrix} \dot{\sigma_1} \\ \dot{\sigma_2} \\ \dot{\sigma_3} \\ \dot{\sigma_4} \\ \dot{\sigma_5} \\ \dot{\sigma_6} \\ \dot{\sigma_7} \end{bmatrix} +$$

$$\frac{\kappa}{\Delta x^2} \begin{bmatrix} 1 & -1 & 0 & 0 & 0 & 0 & 0 \\ -1 & 2 & -1 & 0 & 0 & 0 & 0 \\ 0 & -1 & 2 & -1 & 0 & 0 & 0 \\ 0 & 0 & -1 & 3 & -1 & 0 & -1 \\ 0 & 0 & 0 & -1 & 2 & -1 & 0 \\ 0 & 0 & 0 & 0 & -1 & 1 & 0 \\ 0 & 0 & 0 & -1 & 0 & 0 & 1 \end{bmatrix} \begin{bmatrix} \sigma_1 \\ \sigma_2 \\ \sigma_3 \\ \sigma_4 \\ \sigma_5 \\ \sigma_6 \\ \sigma_7 \end{bmatrix} = \frac{\kappa\beta}{\Delta x} \begin{bmatrix} j_1 \\ 0 \\ 0 \\ -j_1 + j_2 - j_3 \\ 0 \\ -j_2 \\ j_3 \end{bmatrix} \tag{32}$$

Note that if the widths and thicknesses of the three segments are not equal, then these would be part of the BC (3) enforcing continuity of atomic flux at the junction, and thus they would appear in both matrices above.

For a general interconnect tree, the ODE system (32) takes the generalized state-space form:

$$\mathbf{E}\dot{\boldsymbol{\sigma}}(t) + \frac{\kappa}{\Delta x^2}\mathbf{G}\boldsymbol{\sigma}(t) = \frac{\kappa\beta}{\Delta x}\mathbf{D}\mathbf{j} \tag{33}$$

Since the matrix $\mathbf{E}$ is nonsingular and diagonal, it can easily be inverted, leading to the same LTI system form of (22), where $\mathbf{A} = -\frac{\kappa}{\Delta x^2}\mathbf{E}^{-1}\mathbf{G}$ and $\mathbf{B} = \frac{\kappa\beta}{\Delta x}\mathbf{E}^{-1}\mathbf{D}$, and whose solution is given by (24).

If now the segment current densities are assumed constant, and if the matrix $\mathbf{A}$ is nonsingular, it can be shown by integrating the power series expansion of the matrix exponential that the solution (24) can be written analytically (assuming $\boldsymbol{\sigma}(0) = 0$)) as:

$$\boldsymbol{\sigma}(t) = \left(e^{\mathbf{A}t} - \mathbf{I}\right)\mathbf{A}^{-1}\mathbf{B}\mathbf{j} \tag{34}$$

Of course the matrix $\mathbf{A}$ here is singular, since its rows and columns add up to zero, the reason being that the stress equations for discretized points are not independent. One such independent equation relating stresses at all discrete points is the conservation of mass condition (6), whose discretized form and approximation at discrete points (rather than discrete segments) is [26]:

$$\sum_{i=1}^{n}\left(\frac{1}{2}\sum_{s_k \in S_i} w_{s_k}\tau_{s_k}\Delta x\right)\sigma_i = 0 \tag{35}$$

This can be solved with respect to stress at any discrete point (preferably an internal one, e.g. σ_2), and the resulting expression substituted to the other equations of (32) containing this point, so that a $(n-1)\times(n-1)$ ODE system is obtained whose system matrix is now nonsingular. Apart from that, a computational challenge in evaluating (34) is the cost of computing the matrix exponential for large orders of n. Since only the product of the matrix exponential with a vector is needed here, very efficient techniques can be used [39]. Both the above issues were addressed in the work [40].

The works in [41–43] can also fall into the class of semi-analytical approaches. These attempt to analytically solve Korhonen's equation (without space or time discretization) for multisegment interconnect trees by the method of Separation of Variables. However, the application to general interconnect trees requires the calculation of unknown eigenvalues of a matrix with nonlinear functions involving a nonstandard (and rather expensive) numerical algorithm referred to as Wittrick-Williams (along with QR factorization).

Finally, we note purely numerical approaches that discretize time as well as space, and attempt to either solve the complete system with a numerical time integration method [17], or perform model order reduction and solve a reduced-order system [44].

4.4 Mapping EM Stress Analysis to Circuits

Transient analysis typically assumes that each segment in an interconnect carries a constant current density j. As a result, $\partial(\beta j)/\partial x = 0$, and Korhonen's equation (1) for each segment becomes:

$$\frac{\partial\sigma}{\partial t} = \kappa\frac{\partial^2\sigma}{\partial x^2} \tag{36}$$

The above equation is similar to the heat equation, which is often solved under the finite-difference method (FDM) [45]; this was briefly observed earlier in Section 4.1. Under an FDM discretization, the heat equation can be mapped to an electrical circuit where each element corresponds to a node. Adjacent elements are connected by resistors, and capacitors lie between elements and the ground node. The value of the "thermal resistance" depends on the thermal conductivity and the dimensions of the element, while that of the "thermal capacitance" depends on physical constants for the medium and the volume of the element. The excitations to this system are the points where power is dissipated, which are modeled using "thermal current sources" connected to the RC network. We solve for the node voltages in this network, which correspond to the temperature in each element.

A similar analogy may be made for EM stress analysis [46], where the stress corresponds to the node voltages in an equivalent RC circuit. In a modification to the model in [46], the parameter κ maps one-to-one with thermal conductivity and provides the "stress resistance"; the "stress capacitance" depends on the element volume; the excitations correspond to a set of current sources that model currents in the wire segments. Boundary conditions on continuity (2) map naturally to the electrical circuit: end points of adjacent segments are connected to the same node and must have the same voltage (i.e., stress). Flux conditions (3) are captured by appropriately setting the values of the current sources, and mass conservation (6) translates into a requirement that a weighted sum of node voltages is zero. Under this mapping, the stress PDE maps on to an RC electrical circuit that can be solved using standard electrical analysis methods to determine transient stress.

5 CONCLUSION

This paper has presented a summary of recent computationally efficient physics-based approaches to solving the problem of EM analysis of multisegment interconnect wires. Solutions to both the steady-state problem, used to identify immortal wires, and the transient problem, which determines stress evolution as a function of time, are presented. Based on the resurgence of interest in this area, its importance to modern chip design, and the development of fast, linear-time approaches for solving these problems, we anticipate significant developments in this area in the near future. An open question remains as to how physics-based methods can interact with foundry models. This is a topic for future investigation.

Acknowledgments: This work was supported in part by the National Science Foundation under award 1714805 and by SPAWAR under contract N660011824048.

REFERENCES

[1] J. Lienig, "Electromigration and its impact on physical design in future technologies," in *Proceedings of the International Symposium on Physical Design*, pp. 33–40, 2013.

[2] J. Lienig and M. Thiele, "The pressing need for electromigration-aware physical design," in *Proceedings of the International Symposium on Physical Design*, pp. 144–151, 2018.

[3] S. S. Sapatnekar, "Electromigration-aware interconnect design," in *Proceedings of the International Symposium on Physical Design*, pp. 83–90, 2019.

[4] S. M. Alam, *et al.*, "Circuit-level reliability requirements for Cu metallization," *IEEE Transactions on Devices and Materials Reliability*, vol. 5, no. 3, pp. 522–531, 2005.

[5] C. Auth, *et al.*, "A 10nm high performance and low-power CMOS technology featuring 3rd generation FinFET transistors, self-aligned quad patterning, contact over active gate and cobalt local interconnects," in *IEEE International Electronic Devices Meeting*, pp. 29.1.1–29.1.4, 2017.

[6] I. A. Blech, "Electromigration in thin aluminum films on titanium nitride," *Journal of Applied Physics*, vol. 47, no. 4, pp. 1203–1208, 1976.

[7] J. R. Black, "Electromigration failure modes in aluminum metallization for semiconductor devices," *Proceedings of the IEEE*, vol. 57, no. 9, pp. 1587–1594, 1969.

[8] R. Rosenberg and M. Ohring, "Void formation and growth during electromigration in thin films," *Journal of Applied Physics*, vol. 42, no. 13, pp. 5671–5679, 1971.

[9] M. Schatzkes and J. R. Lloyd, "A model for conductor failure considering diffusion concurrently with electromigration resulting in a current exponent of 2," *Journal of Applied Physics*, vol. 59, pp. 3890–3893, 1986.

[10] J. J. Clement and J. R. Lloyd, "Numerical investigations of the electromigration boundary value problem," *Journal of Applied Physics*, vol. 71, pp. 1729–1731, 1992.

[11] M. A. Korhonen, *et al.*, "Stress evolution due to electromigration in confined metal lines," *Journal of Applied Physics*, vol. 73, no. 8, pp. 3790–3799, 1993.

[12] V. Sukharev, "Beyond Black's equation: Full-chip EM/SM assessment in 3D IC stack," *Microelectronic Engineering*, vol. 120, pp. 99–105, 2014.

[13] H.-B. Chen, *et al.*, "Analytical modeling and characterization of electromigration effects for multibranch interconnect trees," *IEEE Transactions on Computer-Aided Design of Integrated Circuits and Systems*, vol. 35, no. 11, pp. 1811–1824, 2016.

[14] Y. J. Park, *et al.*, "New electromigration validation: Via node vector method," in *Proceedings of the IEEE International Reliability Physics Symposium*, pp. 698–704, 2010.

[15] V. Mishra and S. S. Sapatnekar, "Predicting electromigration mortality under temperature and product lifetime specifications," in *Proceedings of the ACM/IEEE Design Automation Conference*, pp. 43:1–43:6, 2016.

[16] V. Sukharev, *et al.*, "Postvoiding stress evolution in confined metal lines," *IEEE Transactions on Devices and Materials Reliability*, vol. 16, no. 1, pp. 50–60, 2016.

[17] S. Chatterjee, *et al.*, "Power grid electromigration checking using physics-based models," *IEEE Transactions on Computer-Aided Design of Integrated Circuits and Systems*, vol. 37, pp. 1317–1330, July 2018.

[18] H.-B. Chen, *et al.*, "Analytical modeling of electromigration failure for VLSI interconnect tree considering temperature and segment length effects," *IEEE Transactions on Devices and Materials Reliability*, vol. 17, no. 4, pp. 653–666, 2017.

[19] V. Mishra and S. S. Sapatnekar, "The impact of electromigration in copper interconnects on power grid integrity," in *Proceedings of the ACM/IEEE Design Automation Conference*, pp. 88:1–88:6, 2013.

[20] B. Li, *et al.*, "Statistical evaluation of electromigration reliability at chip level," *IEEE Transactions on Devices and Materials Reliability*, vol. 11, pp. 86–91, Mar. 2011.

[21] J. Gambino, "Process technology for copper interconnects," in *Handbook of Thin Film Deposition* (K. Seshan and D. Schepis, eds.), ch. 6, pp. 147–194, Amsterdam, The Netherlands: Elsevier, 3rd ed., 2018.

[22] L. Zhang, *et al.*, "Grain size and cap layer effects on electromigration reliability of cu interconnects: Experiments and simulation," in *AIP Conference Proceedings*, vol. 1300, 3, 2010.

[23] S. P. Riege, *et al.*, "A hierarchical reliability analysis for circuit design evaluation," *IEEE Transactions on Electron Devices*, vol. 45, pp. 2254–2257, Oct. 1998.

[24] J. J. Clement, *et al.*, "Methodology for electromigration critical threshold design rule evaluation," *IEEE Transactions on Computer-Aided Design of Integrated Circuits and Systems*, vol. 18, pp. 576–581, May 1999.

[25] H. Haznedar, *et al.*, "Impact of stress-induced backflow on full-chip electromigration risk assessment," *IEEE Transactions on Computer-Aided Design of Integrated Circuits and Systems*, vol. 25, pp. 1038–1046, June 2006.

[26] E. Demircan and M. Shroff, "Model based method for electro-migration stress determination in interconnects," in *Proceedings of the IEEE International Reliability Physics Symposium*, pp. IT5.1–IT5.6, 2014.

[27] P. Gibson, *et al.*, "Electromigration analysis of full-chip integrated circuits with hydrostatic stress," in *Proceedings of the IEEE International Reliability Physics Symposium*, pp. IT.2.1–IT.2.7, 2014.

[28] F. Najm and V. Sukharev, "Electromigration simulation and design considerations for integrated circuit power grids," *Journal of Vacuum Science & Technology B*, vol. 38, pp. 063204:1–12, Nov/Dec 2020.

[29] M. A. A. Shohel, *et al.*, "A new, computationally efficient 'Blech criterion' for immortality in general interconnects," in *Proceedings of the ACM/IEEE Design Automation Conference*, 2021.

[30] M. A. A. Shohel, *et al.*, "A linear-time algorithm for steady-state analysis of electromigration in general interconnects," in *arXiv:2112.13451 [cs.AR]*, 2021.

[31] Z. Sun, *et al.*, "Fast electromigration immortality analysis for multisegment copper interconnect wires," *IEEE Transactions on Computer-Aided Design of Integrated Circuits and Systems*, vol. 37, pp. 3137–3150, Dec. 2018.

[32] M. A. A. Shohel, *et al.*, "Analytical modeling of transient electromigration stress based on boundary reflections," in *Proceedings of the IEEE/ACM International Conference on Computer-Aided Design*, 2021.

[33] O. Axelou, *et al.*, "A novel semi-analytical approach for fast electromigration stress analysis in multi-segment interconnects," in *Proceedings of the IEEE/ACM International Conference on Computer-Aided Design*, 2022.

[34] K. Daloukas, *et al.*, "Parallel fast transform-based preconditioners for large-scale power grid analysis on graphics processing units (gpus)," *IEEE Transactions on Computer-Aided Design of Integrated Circuits and Systems*, vol. 35, no. 10, pp. 1653–1666, 2016.

[35] C. Van Loan, *Computational Frameworks for the Fast Fourier Transform.* USA: Society for Industrial and Applied Mathematics, 1992.

[36] H. Qian and S. S. Sapatnekar, "Fast poisson solvers for thermal analysis," in *2010 IEEE/ACM International Conference on Computer-Aided Design (ICCAD)*, pp. 698–702, 2010.

[37] S. R. Nassif, "Power grid analysis benchmarks," in *Proceedings of the Asia-South Pacific Design Automation Conference*, pp. 376–381, 2008.

[38] K.-D. Lee, "Electromigration recovery and short lead effect under bipolar- and unipolar-pulse current," in *Proceedings of the IEEE International Reliability Physics Symposium*, pp. 6B.3.1–6B.3.4, 2012.

[39] A. H. Al-Mohy and N. Higham, "Computing the action of the matrix exponential, with an application to exponential integrators," *SIAM Journal of Scientific Computing*, vol. 33, no. 2, pp. 488–511, 2011.

[40] P. Stoikos, *et al.*, "A fast semi-analytical approach for transient electromigration analysis of interconnect trees using matrix exponential," in *Proceedings of the Asia-South Pacific Design Automation Conference*, 2023.

[41] L. Chen, *et al.*, "Fast analytic electromigration analysis for general multisegment interconnect wires," *IEEE Transactions on Very Large Scale Integration (VLSI) Systems*, vol. 28, no. 2, pp. 421–432, 2019.

[42] L. Chen, *et al.*, "A fast semi-analytic approach for combined electromigration and thermomigration analysis for general multisegment interconnects," *IEEE Transactions on Computer-Aided Design of Integrated Circuits and Systems*, vol. 40, no. 2, pp. 350–363, 2021.

[43] X. Wang, *et al.*, "Fast physics-based electromigration analysis for full-chip networks by efficient eigenfunction-based solution," *IEEE Transactions on Computer-Aided Design of Integrated Circuits and Systems*, vol. 40, no. 3, pp. 507–520, 2021.

[44] C. Cook, *et al.*, "Fast electromigration stress evolution analysis for interconnect trees using Krylov subspace method," *IEEE Transactions on VLSI Systems*, vol. 26, no. 5, pp. 969–980, 2018.

[45] M. N. Özişik, *Heat Transfer: A Basic Approach.* New York, NY: McGraw-Hill, 1985.

[46] F. N. Najm, "Equivalent circuits for electromigration," *Microelectronics Reliability*, pp. 114200–1–114200–16, Aug. 2021.